Computers and Mathematics with Applications 79 (2020) 1619–1633

Contents lists available at ScienceDirect

Computers and Mathematics with Applications

journal homepage: www.elsevier.com/locate/camwa

A numerical study of the higher-dimensional Gelfand-Bratu model

Sehar Iqbal *, Paul Andries Zegeling

Department of Mathematics, Faculty of Science, Utrecht University, Netherlands

ARTICLE INFO

Article history:
Received 1 June 2019
Received in revised form 14 September 2019
Accepted 20 September 2019
Available online 9 October 2019

Keywords:
Boundary-value problems
Bratu problem
Finite differences
Bifurcation behaviour
Nonlinear multigrid

ABSTRACT

In this article, a higher dimensional nonlinear boundary-value problem, viz., Gelfand-Bratu (GB) problem, is solved numerically. For the three-dimensional case, we present an accurate and efficient nonlinear multigrid (MG) approach and investigate multiplicities depending on the bifurcation parameter λ. We adopt a nonlinear MG approach *Full approximation scheme* (FAS) extended with a Krylov method as a smoother to handle the computational difficulties for obtaining the upper branches of the solutions. Further, we examine the numerical bifurcation behaviour of the GB problem in 3D and identify the existence of *two* new bifurcation points. Experiments illustrate the convergence of the numerical solutions and demonstrate the effectiveness of the proposed numerical strategy for all parameter values $\lambda \in (0, \lambda_c]$. For higher dimensions, we transform the GB problem, using n-dimensional spherical coordinates, to a nonlinear ordinary differential equation (ODE). The numerical solutions of this nonlinear ODE are computed by a shooting method for a range of values of the dimension parameter n. Numerical experiments show the existence of several types of solutions for different values of n and λ. These results confirm the bifurcation behaviour of the higher dimensional GB problem as predicted from theoretical results in literature.

1. Introduction

In the present article, we consider a higher dimensional nonlinear elliptic boundary-value problem: the Gelfand–Bratu (GB) model [1–3] which depends heavily on the parameter λ. This model coupled with appropriate boundary conditions is used to model the temperature distribution in fuel ignition problems [4]. The GB model simulates also a thermal reaction process in a rigid material where the process depends on the balance between chemically generated heat and heat transfer by conduction [5,6]. The three-dimensional model is considered in investigations on the sun core temperatures [6,7]. The GB model appears in several contexts such as thermo-electro-hydrodynamics models [8] and elasticity theory [9].

In literature, only a few numerical methods have been proposed for the GB model in higher dimensions. For the three-dimensional GB model, only two solutions (lower and upper) are presented by using nonstandard compact finite difference scheme in [10]. A pseudospectral method, finite difference method and radial basis functions method for the three-dimensional GB problem, are discussed in [11] which illustrates the bifurcation behaviour in detail. On the unit ball, the GB model is investigated numerically in which the solution dependence on the parameter λ for all dimension parameter n is described in [12] and radially symmetry is demonstrated in [13]. Three-dimensional bifurcation diagrams on a ball and annular domains are discussed with the help of a pseudo-arclength continuum method in [14].

* Corresponding author.
E-mail address: s.iqbal@uu.nl (S. Iqbal).

https://doi.org/10.1016/j.camwa.2019.09.018
0898-1221/

In this work, we show numerical convergence to different types of solutions and present a bifurcation curve for the GB model in higher dimensions. We focus our research to positive solutions for $\lambda > 0$. For the numerical computation of the three-dimensional GB model, we have chosen to use a nonlinear multigrid approach. This multigrid approach can be applied directly to the nonlinear elliptic equations without the use of a global linearization technique. This is known as *full approximation schemes* (FAS). In FAS multigrid, linearization of the nonlinear problem is treated locally in the relaxation step on different grid sizes. It is well known that the FAS multigrid idea is based on two principles: an error smoothing on fine grids and then followed by coarse grid corrections. In this work, we concentrate on the computational difficulties such as a possible unstable convergence behaviour and the loss of diagonal dominance of the Jacobian matrix for obtaining the upper branches of solutions of the GB model by FAS multigrid approach. The Jacobian matrix depends on the solution values, the parameter λ and the grid size h. To handle these difficulties, we use a MINRES method as a smoother in FAS multigrid approach instead of a classical smoother (Gauss–Seidel method). This multigrid approach solves successfully the problems of the Jacobian matrix for large values of the solutions, which correspond to the upper solution branches. The main contribution of the present work in the three-dimensional GB model, is to compute accurately multiple solutions and to confirm the numerical convergence of the upper branches of solutions for all values of $\lambda \in (0, \lambda_c]$. Furthermore, we investigate the numerical bifurcation behaviour of the GB problem in three dimensions and identify the existence of two new turning points. As known from the literature [11,14], finding multiple solutions and new turning points for higher dimensions in the GB problem is a hard task. Our numerical results illustrate the accuracy and efficiency of the proposed multigrid approach.

For even higher space dimensions (greater than three), we transform the GB problem using n-dimensional spherical coordinates to a nonlinear ordinary differential equation (ODE). The numerical solutions of this nonlinear ODE are computed by a shooting method for a range of values of the dimension parameter n. We compute several types of solutions of the GB model on an n-dimensional ball B for different values of n and λ. All multiple solutions of the nonlinear ODE on the ball B can be proved to be positive, because of the maximum principle and radial symmetry (for more details, see [4]). In the present work, we numerically confirm the existence of multiple solutions depending on the parameters n and λ. Numerical results clarify the bifurcation curves in the higher dimensional GB problem obtained from theoretical results in literature [4].

The article is organized as follows. In Section 2, we describe the GB problem in n space dimensions. Section 3 is devoted to the discretization of the n-dimensional Laplacian. In Section 4, the three-dimensional GB model is discussed, where in the nonlinear multigrid approach FAS is used to compute the numerical results and illustrate the multiplicity of solutions in detail. The GB model for higher dimensions is discussed in Section 5, which incorporate a coordinate transformation from Cartesian to n-dimensional spherical coordinates to obtain a nonlinear ODE on a unit ball $B \subset \mathbb{R}^n$. Numerical experiments show several types of solutions and create bifurcation diagrams. The concluding remarks are presented in Section 6.

2. A boundary-value problem in n space dimensions

Consider the following nonlinear elliptic boundary-value problem, also known as the n-dimensional GB model:

$$\begin{aligned} \Delta u(\vec{\mathrm{x}}) + \lambda\, \mathrm{e}^{u(\vec{\mathrm{x}})} = 0, \qquad & \mathrm{x} \in \Omega = [0,1]^n \subset \mathbb{R}^n, \\ u(\vec{\mathrm{x}}) = 0, \qquad & \vec{\mathrm{x}} \in \partial\Omega, \end{aligned} \tag{1}$$

where $\lambda > 0$, $\vec{\mathrm{x}} = (x_1, x_2, x_3, \ldots, x_n)^T$ and the Laplacian operator Δ in n-dimensions is given by:

$$\Delta = \sum_{k=1}^{n} \frac{\partial^2}{\partial x_k^2}.$$

3. Discretization of the Laplacian in n space dimensions

For the numerical solution of model (1), we work out a central finite difference scheme for the n-dimensional Laplacian. On a uniform grid on the domain Ω, we generate the grid points by

$$(\mathrm{x}_i)_j = jh, \quad \text{with} \quad h = \tfrac{1}{J}, \quad i = 1, 2, \ldots, n, \quad j = 0, 1, 2, \ldots, J.$$

We write $u_{i_1,i_2,i_3,\ldots,i_n}$ to represent the discrete approximation of the exact (unknowns) values $u(x_1, x_2, x_3, \ldots, x_n)$. A second-order central finite difference approximation for dimensions $1, 2, \ldots, n$ reads, respectively:

$$1d: \quad \Delta u|_{i_1} = u_{xx}|_{i_1} \approx \frac{1}{h^2}(u_{i_1+1} + u_{i_1-1} - 2u_{i_1})$$

$$2d: \quad \Delta u|_{i_1,i_2} = u_{x_1x_1}|_{i_1,i_2} + u_{x_2x_2}|_{i_1,i_2} \approx \frac{1}{h^2}(u_{i_1+1,i_2} + u_{i_1-1,i_2} + u_{i_1,i_2+1} + u_{i_1,i_2-1} - 4u_{i_1,i_2}),$$

$$\begin{aligned} 3d: \quad \Delta u|_{i_1,i_2,i_3} &= u_{x_1x_1}|_{i_1,i_2,i_3} + u_{x_2x_2}|_{i_1,i_2,i_3} + u_{x_3x_3}|_{i_1,i_2,i_3} \\ &\approx \frac{1}{h^2}(u_{i_1+1,i_2,i_3} + u_{i_1-1,i_2,i_3} + u_{i_1,i_2+1,i_3} + u_{i_1,i_2-1,i_3} + u_{i_1,i_2,i_3+1} + u_{i_1,i_2,i_3-1} - 6u_{i_1,i_2,i_3}), \end{aligned}$$

$$\vdots$$

$$nd: \ \Delta u|_{i_1,i_2,i_3\ldots i_n} \approx \frac{1}{h^2}\underbrace{(u_{i_1+1,i_2,i_3,\ldots,i_n} + u_{i_1-1,i_2,i_3,\ldots,i_n} + \ldots + u_{i_1,i_2,i_3,\ldots,i_n+1} + u_{i_1,i_2,i_3,\ldots,i_n-1}}_{2n \text{ terms}}$$
$$- \ 2n\, u_{i_1,i_2,i_3,\ldots,i_n}).$$

4. The three-dimensional case

In this section, we treat the three-dimensional (3D) case ($n = 3$). The main goal is to numerically determine the multiple existence of solutions for a given bifurcation parameter $\lambda > 0$ on the domain $[0, 1]^3$. Another objective is to show the convergence of these numerical solutions with the aid of an efficient numerical method.

4.1. Numerical method

The nonlinear boundary-value problem (1) is discretized by a seven-point finite difference formula on a uniform grid with step size h. The resulting nonlinear system of equations becomes:

$$\frac{1}{h^2}(u_{i_1+1,i_2,i_3} + u_{i_1-1,i_2,i_3} + u_{i_1,i_2+1,i_3} + u_{i_1,i_2-1,i_3} + u_{i_1,i_2,i_3+1} + u_{i_1,i_2,i_3-1} - 6u_{i_1,i_2,i_3}) + \lambda\, e^{u_{i_1,i_2,i_3}} = 0, \tag{2}$$

where u_{i_1,i_2,i_3} is the approximation at $(x_{i_1}, x_{i_2}, x_{i_3})$, $1 \le i_1, i_2, i_3 \le J - 1$. The Dirichlet boundary conditions read:

$$u_{0,i_2,i_3} = u_{J,i_2,i_3} = u_{i_1,0,i_3} = u_{i_1,J,i_3} = u_{i_1,i_2,0} = u_{i_1,i_2,J} = 0.$$

We present a multigrid approach for solving the discretized system of nonlinear equations (2). This approach is known as the *Full Approximation Storage* (FAS), where the system of equations (2) is solved on each level of the grid throughout the multigrid cycle. For large values of the solution u, which could be the case when we look for multiple solutions, diagonal dominance of the tridiagonal matrix is lost. As a result, the tridiagonal matrix may become indefinite on coarser grids. Thus in such cases, standard smoothers such as Gauss–Seidel become unstable. To handle such a difficulty, the MINRES-method (a Krylov subspace method) is introduced as a smoother instead of a Gauss–Seidel method. Next, we describe the numerical strategy to compute multiple solutions for $\lambda \in (0, \lambda_c]$. Recall that the nonlinear discretized system of equations (2) on the original fine grid with step size $h = \frac{1}{J}$ on the domain $[0, 1]^3$ can be written as:

$$N_h(u_h) = 0, \tag{3}$$

where $N_h(.)$ is the discretized nonlinear operator $N(u) = Au + \lambda e^u$. Let $\tilde{u}_h$ be the approximate solution on the fine grid h of the nonlinear system (2). Restrict the fine grid residual r_h to the coarse grid residual r_{2h} by the restriction operator R_h^{2h}. We iterate system (2) for $\tilde{u}_{2h}$ on the coarse grid $2h$ to approximate the coarse grid error e_{2h}. Interpolate e_{2h} back to the fine grid error e_h by using the interpolating operator I_{2h}^h. Make the correction of the fine grid solution as $\tilde{u}_h + e_h$ (see Algorithm 1). This fine-coarse-fine loop is a two-grid V-cycle (we denote it by *V-cycle*) is continued until the tolerance is obtained. Assume that ν_1 and ν_2 are the pre-smoothing and post-smoothing steps respectively. The complete *FAS* two grid V-Cycle algorithm is explained as:

Algorithm 1: FAS V-cycles

1. Relax ν_1 times, to compute $\tilde{u}_h$ by using smoother with initial guess $\tilde{u}_h^0$.
2. Compute the residual on fine grid: $r_h = 0 - N_h(\tilde{u}_h)$.
3. Restrict the residual: $r_{2h} = -R_h^{2h} r_h$.
4. Inject the solution $\tilde{u}_{2h}^{init} = I_h^{2h} \tilde{u}_h$.
5. If coarsest grid then solve $N_{2h}(\tilde{u}_{2h}) = N_{2h}(\tilde{u}_{2h}^{init}) - r_{2h}$ exactly,
else, call γ times the *FAS* scheme recursively.
6. Calculate the coarse grid error $e_{2h} = \tilde{u}_{2h} - \tilde{u}_{2h}^{init}$.
7. Interpolate the error back on fine grid: $e_h = I_{2h}^h e_{2h}$.
8. Correct the fine grid solution: $\tilde{u}_h + e_h$.
9. Relax ν_2 times, starting from the improved $\tilde{u}_h$ as nonlinear smoother.

Here, the unknown solution u is relaxed by the *MINRES* method as a smoother for the discretized linearized equation [15,16]. The linearized equation for the nonlinear boundary-value problem (1) becomes:

$$\Delta u + \lambda\, f(\tilde{u})\, u = \lambda\, (\tilde{u} - 1)\, f(\tilde{u}),$$

where $\tilde{u}$ is the current approximate solution of u (mentioned also in step 1 of the Algorithm).

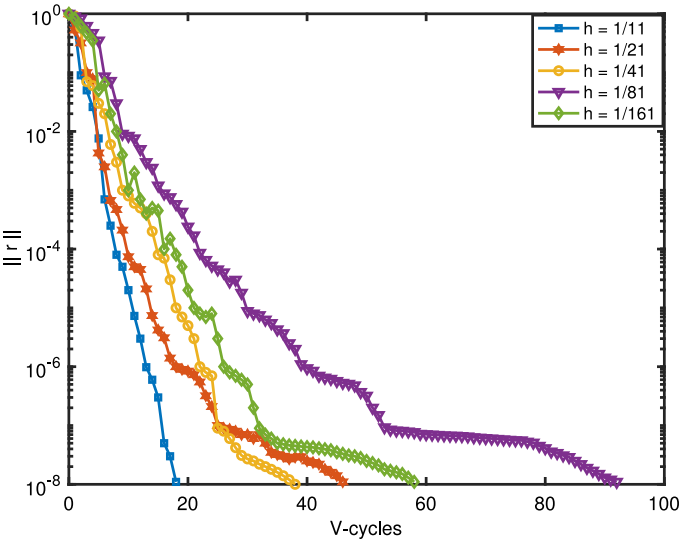

Fig. 1. Numerical convergence for a single solution of the three-dimensional GB model (1) for $\lambda = 0.1$ on decreasing grid sizes h.

4.2. Numerical results

In this section, we discuss the numerical implementation of the proposed numerical method for model (1) in 3D. We examine the performance of the FAS-MG by using MINRES method as a smoothing relaxation with an appropriate initial guess. We observed that the proposed multigrid method is very sensitive to the initial guess, particularly for different values of λ, near to λ_c and for both turning points: λ_a, λ_b for small h. The FAS multigrid approach cannot perform efficiently, since the coarse grids can not provide an accurate approximation to the solution. In order to make the scaling independent of the grid size h, the following residual norm is defined in the numerical procedure:

$$\|r\|_2 = \sqrt{\frac{\sum_{i_1,i_2,i_3} r^2_{i_1,i_2,i_3}}{J}}. \tag{4}$$

We choose the initial approximation on the fine grid h as follows:

$$u_{initial} = u^0 = \alpha \sin(k\pi x_{i_1}) \sin(k\pi x_{i_2}) \sin(k\pi x_{i_3}) \tag{5}$$

with an amplitude α and frequency k. These numerical parameters must be specified for each experiment separately. The stopping criteria that we use is: $\|r\|_2 \leq 10^{-8}$. We choose the multigrid cycle $V(2,2)$ and the coarse grid of size $h = \frac{1}{2}$ with one interior node. We examine the bifurcation behaviour by illustrating the existence of multiple solutions for different values of λ. Numerical results also provide the convergence for all $\lambda \in (0, \lambda_c]$ on different grids with size h. This shows that the proposed numerical strategy is more accurate and efficient than the other numerical techniques in [11,14] to find the lower and upper solutions of model (1) in 3D.

4.2.1. Multiplicity of solutions

One of the goals of the present numerical study is to compute multiple solutions for the three-dimensional case. Note that the numerical solutions depend heavily on the parameter λ and grid size h. The proposed numerical method worked very well for all $\lambda \in (0, \lambda_c]$ which is one of the main contributions of the present work. Table 1 shows the maximum value of the first: u_1, second: u_2, third: u_3 and fourth: u_4 solutions for different values of $\lambda > 0$ with $h = 1/161$. In Table 1, the numerical solution with $*$ indicates that the solution does not converge for the given tolerance on a grid with a high number of grid points J.

4.2.2. Numerical convergence in the case of multiple solutions

The convergence of the numerical solutions, especially for the solutions u_2, u_3, u_4, is of great importance as it confirms the existence of more than two solutions. It is the first time, as far as we know, that the numerical convergence of these multiple solutions on small grids size is described. With the help of FAS-MG, we successfully obtain numerical convergence for both small values of λ and the new bifurcation points λ_a, λ_b as well as for the critical value λ_c. All these aspects of the numerical convergence for different values of λ for a large number of grid points J are discussed in detail. For the small parameter value: $\lambda = 0.1$, Fig. 1 shows the numerical convergence of the solution on different grid sizes. It shows the effectiveness of the FAS-MG method for the GB model in 3D. For $\lambda \in (0, \lambda^b)$, we are able to compute two solutions,

Table 1
The maximum value of the solutions of the three-dimensional GB model (1) for $\lambda > 0$ and $h = 1/161$.

λ	u_1	u_2	u_3	u_4
$\lambda_c \approx 9.90257408$	1.576134	–	–	–
9.5	1.164208	2.355216	–	–
8.0	0.765826	3.357463	–	–
6.5	0.515261	4.026373	–	–
$\lambda_a \approx 6.31432062$	0.491024	4.188615	6.246388	–
6.2	0.488463	4.065204	5.903662	6.601146
6.1	0.462888	4.142452	5.802547	6.663853
6.0	0.467853	4.184735	5.885483	6.724115
5.9	0.455032	4.213302	5.813532	6.767654*
5.5	0.405615	4.496710	5.631087	6.973204*
$\lambda_b \approx 4.8261277$	0.326448	5.163705	7.1683172*	–
4.8	0.321485	–	7.198551*	–
4.5	0.311926	7.244282*	–	–
2.0	0.124607	7.600145*	–	–
1.5	0.089335	7.812563*	–	–
f1.0	0.056903	8.162511*	–	–
0.5	0.028631	–	–	–
0.3	0.008993	–	–	–
0.1	0.007436	–	–	–

*Indicates that no numerical convergence was reached.

Table 2
The number of V-cycles and the CPU time for the first solution of the three-dimensional GB model (1) with $\lambda = 1$ on decreasing values of grid sizes h.

Grid size	First solution		Second solution	
h	V-cycles	Time (s)	V-cycles	Time (s)
1/11	8	66.2208	48	796.1986
1/21	12	186.2955	100*	1044.4375
1/41	12	432.4789	100*	1331.5509
1/81	18	805.0368	100*	1905.0087
1/161	16	1416.9937	100*	2643.6743

*Indicates that no numerical convergence was reached.

Table 3
The number of V-cycles and the CPU time for the first and second solutions of the three-dimensional GB model (1) for $\lambda = 5.5$ on decreasing values of h.

Grid size	First-solution		Second-solution	
h	V-cycles	Time (s)	V-cycles	Time (s)
1/11	8	41.8657	28	158.9705
1/21	12	118.0548	22	293.3296
1/41	8	288.6603	48	576.2328
1/81	12	443.5499	36	825.5191
1/161	18	757.4487	42	1196.1645

in which the first solution has converged for small values of h, whereas the second solution is a spurious solution (See Table 1). To explain this convergence behaviour we take $\lambda = 1$ as a characteristic example. The numerical convergence of both solutions for $\lambda = 1$ is given in Table 2. Fig. 2 demonstrates that the proposed method successfully converges to the unique solution for the critical value of λ_c on fine grids. For both new bifurcation turning points $\lambda_a \approx 6.31432062$ and $\lambda_b \approx 4.82612776$, three solutions are obtained (for λ_b there is one spurious solution). For λ_a all solutions u_1, u_2, u_3 have numerically converged on a large number of grid points J as shown in Fig. 3. However, for λ_b, one of the solutions, viz., u_3 did not converge on a fine grid (see in Fig. 4).

For $\lambda \in (\lambda_b, \lambda_a)$, we are able to compute *four* numerical solutions. In particular, the computation of the fourth solution, is a difficult task, as MG-methods are very sensitive to the choice of the initial guess. However, the FAS-MG method efficiently resolved the computational difficulties with the MINRES method as a smoother and with an appropriate initial guess. It is important to mention that the proposed MG-method successfully achieved convergence for all $\lambda \in (0, \lambda_c]$. To demonstrate the existence of the *three* solutions, we present the numerical convergence of such solutions u_1, u_2 and u_3 for $\lambda = 5.5$. This is shown in Tables 3, 4. Fig. 5 shows the isosurface plots of the three solutions for $\lambda = 5.5$ on a grid with 41^3 grid points.

To illustrate the existence of a *fourth* solution, we take $\lambda = 6$ as a characteristic example. Fig. 6 presents the isosurface plots of the four solutions: u_1, u_2, u_3, u_4 for $\lambda = 6$ on a grid with 41^3 grid points. Numerical convergence is confirmed in Fig. 7.

Table 4
The number of V-cycles and the CPU time for the third and fourth spurious solution of the three-dimensional GB model (1) for $\lambda = 5.5$ and decreasing values of h.

Grid size	Third-solution		Fourth-solution	
h	V-cycles	Time (s)	V-cycles	Time (s)
1/11	36	242.3997	72	707.5586
1/21	46	426.2311	100*	1494.4805
1/41	42	974.5904	100*	1857.3858
1/81	52	1506.6630	100*	2643.1886
1/161	86	2133.0085	100*	3326.8374

*Indicates that no numerical convergence was reached.

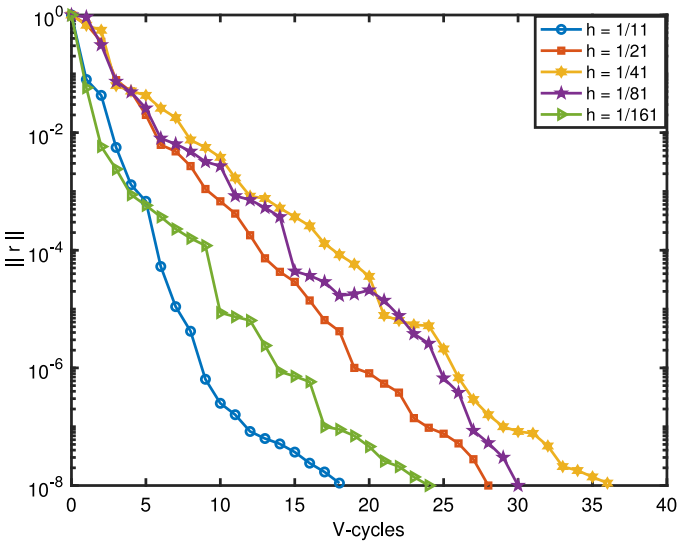

Fig. 2. Numerical convergence for the unique solution of the three-dimensional GB model (1) for the critical value λ_c on decreasing values of h.

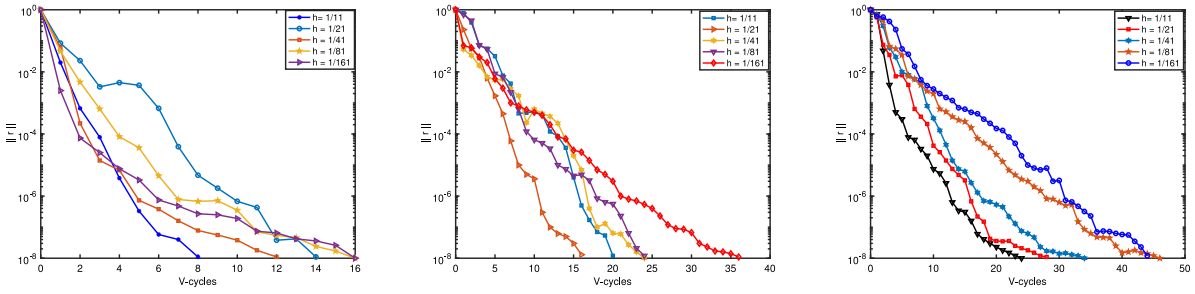

(a) first solution: u_1 (b) second solution: u_2 (c) third solution: u_3

Fig. 3. Numerical convergence of the three solutions: first solution: u_1 (left), second solution: u_2 (middle) and third solution: u_3 (right), respectively, for $\lambda_a \approx 6.31432062$ on decreasing values of grid sizes h of the three-dimensional GB model.

4.2.3. A bifurcation curve in three space dimensions

Our numerical investigations for $\lambda \in (0, \lambda_c]$ give rise to a qualitative picture of the bifurcation curve in three space dimensions for model (1), which is quite different from the one and two-dimensional case. For the three-dimensional case, we present the bifurcation curve in Fig. 8, where two new turning points $\lambda_a \approx 6.31432062$ and $\lambda_b \approx 4.8261277$ are identified. Different numerical experiments for the values of λ lead to the numerical value $\lambda_c \approx 9.90257408$. Fig. 8 incorporates the four solutions, two new turning points and one critical point for $\lambda \in (0, \lambda_c]$. In three dimensions, it can be seen clearly that for $\lambda \geq 6$ we found four solutions (denoted by "4th $-$ *solution* solid line") and for $\lambda \leq 5.9$, one solution out of the four solutions is a spurious one (denoted by "4th $-$ *solution** dashed-line") within (λ_b, λ_a).

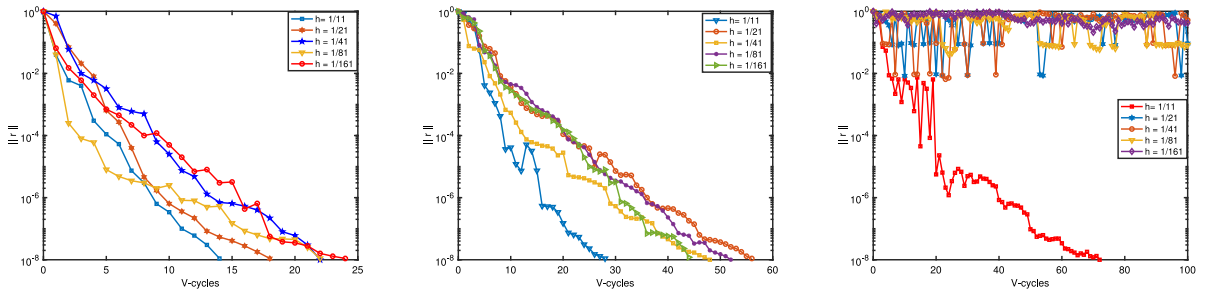

(a) first solution: u_1 (b) second solution: u_2 (c) third spurious solution*: u_3^*

Fig. 4. Numerical convergence of two solutions: first solution: u_1 (left), second solution: u_2 (middle) and divergence of the third spurious solution: u_3^* (right), respectively, for $\lambda_b \approx 4.82612776$ and decreasing values of grid sizes h of the three-dimensional GB model.

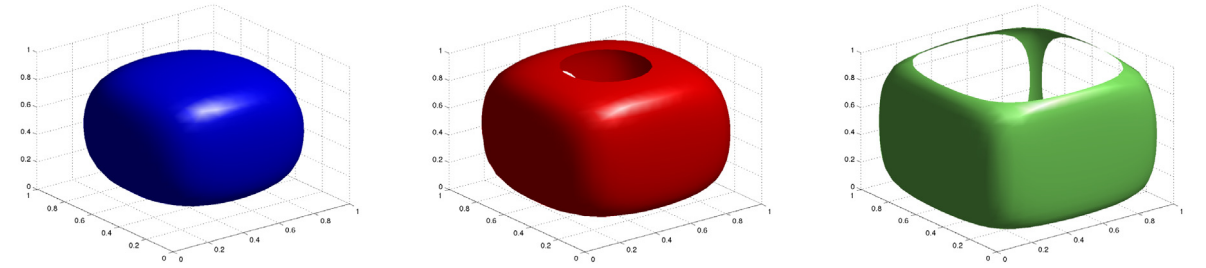

(a) first solution: u_1 (b) second solution: u_2 (c) third solution: u_3

Fig. 5. Iso-surface plots of three solutions: u_1, u_2 and u_3, respectively, of model (1) in three space dimensions for $\lambda = 5.5$ at the iso-value $= 0.35$.

5. The n-dimensional radial case

Motivated by the three-dimensional numerical results in Cartesian coordinates, we will now investigate the multiplicity of solutions and the bifurcation behaviour in n space dimensions. In this section, we look for multiple solutions of nonlinear BVP (1) on a special domain Ω, viz., the n-dimensional ball $B := \{\vec{x} \in \mathbb{R}^n : \|\vec{x}\|_2 < 1\}$. For this, we first transform model (1) using n-dimensional spherical coordinates. All solutions of (1) on B can be proved to be positive, because of the maximum principle and the radial symmetry (for more details, see [4]). We transform the equation from Cartesian coordinates to n-dimensional spherical coordinates. After that we compute numerical solutions of the n-dimensional nonlinear problem in spherical coordinates.

5.1. Spherical coordinates in n space dimensions

In this section, we transform the equation in n space dimensions from Cartesian coordinates $(x_1, x_2, x_3, \ldots, x_n)$ to (hyper-)spherical coordinates $(\rho, \phi_1, \phi_2, \phi_3, \ldots, \phi_{n-1})$ and investigate radially symmetric solutions of nonlinear BVP (1). In Cartesian coordinates, which are mainly useful for rectangular domains, the Laplace operator has the form:

$$\Delta = \sum_{k=1}^{n} \frac{\partial^2}{\partial x_k^2}. \tag{6}$$

For more complicated domains, it is convenient to work with other coordinate systems. A general, so-called curvilinear, coordinate system can be written as follows:

$$\begin{cases} x_1 = x_1(q_1, q_2, q_3, \ldots, q_n), \\ x_2 = x_2(q_1, q_2, q_3, \ldots, q_n), \\ x_3 = x_3(q_1, q_2, q_3, \ldots, q_n), \\ \vdots \\ x_n = x_n(q_1, q_2, q_3, \ldots, q_n), \end{cases} \tag{7}$$

where $(q_1, q_2, q_3, \ldots, q_n)$ are orthogonal curvilinear coordinates and $(x_1, x_2, x_3, \ldots, x_n)$ Cartesian coordinates, respectively.

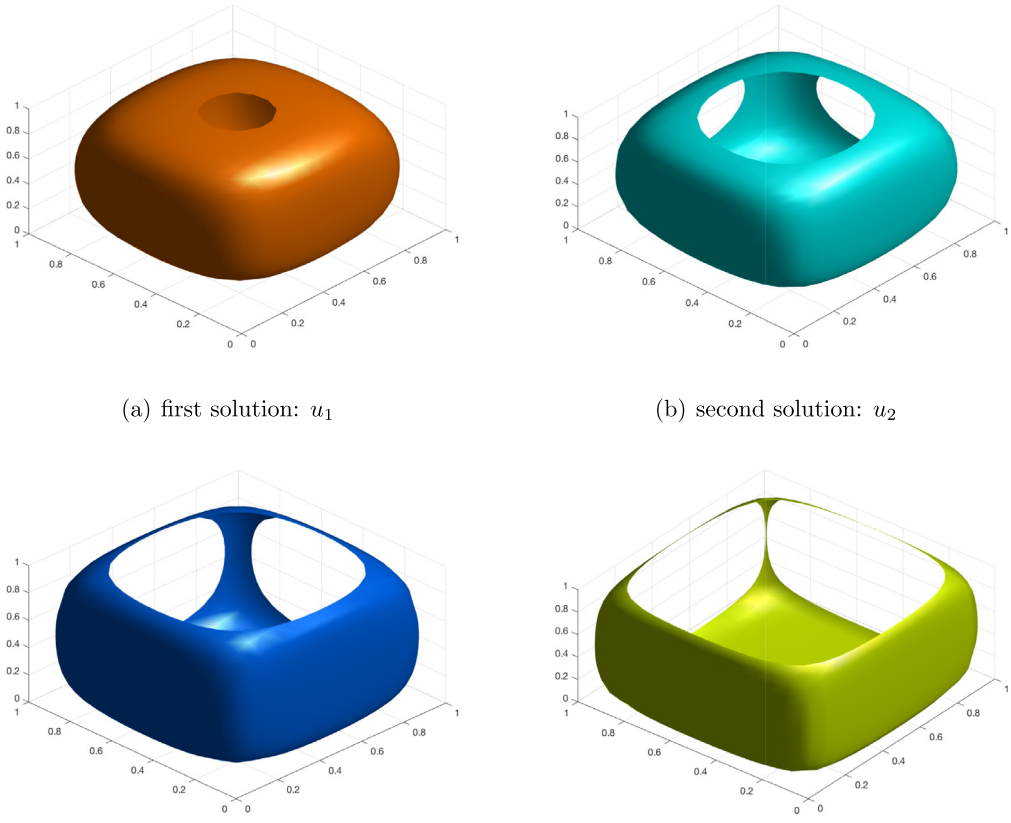

(a) first solution: u_1 (b) second solution: u_2

(c) third solution: u_3 (d) fourth solution: u_4

Fig. 6. Iso-surface plots of four solutions of the three-dimensional GB model (1) for $\lambda = 6.0$ at the iso-value $= 0.42$.

By considering Eq. (7), we can write the tangent vectors to the curvilinear coordinates in terms of scale coefficients and unit vectors as:

$$\sum_{k=1}^{n} \frac{\partial x_k}{\partial q_j} = \zeta_j \, \mathbf{e}_j, \qquad j = 1, 2, \ldots, n,$$

where $\mathbf{e}_j$ are the unit vectors in the direction of the curvilinear coordinates q_j, respectively. The scaling coefficient ζ is defined as:

$$\zeta = \prod_{j=1}^{n} \zeta_j,$$

where

$$\zeta_j = \left[\sum_{k=1}^{n} \left(\frac{\partial x_k}{\partial q_j} \right)^2 \right]^{1/2}, \qquad j = 1, 2, 3, \ldots, n.$$

Then, a general expression for the Laplacian Δ in orthogonal curvilinear coordinates is of the form (see also [17]):

$$\Delta = \frac{1}{\zeta} \sum_{k=1}^{n} \frac{\partial}{\partial q_k} \left(\frac{\zeta}{\zeta_k^2} \frac{\partial}{\partial q_k} \right). \tag{8}$$

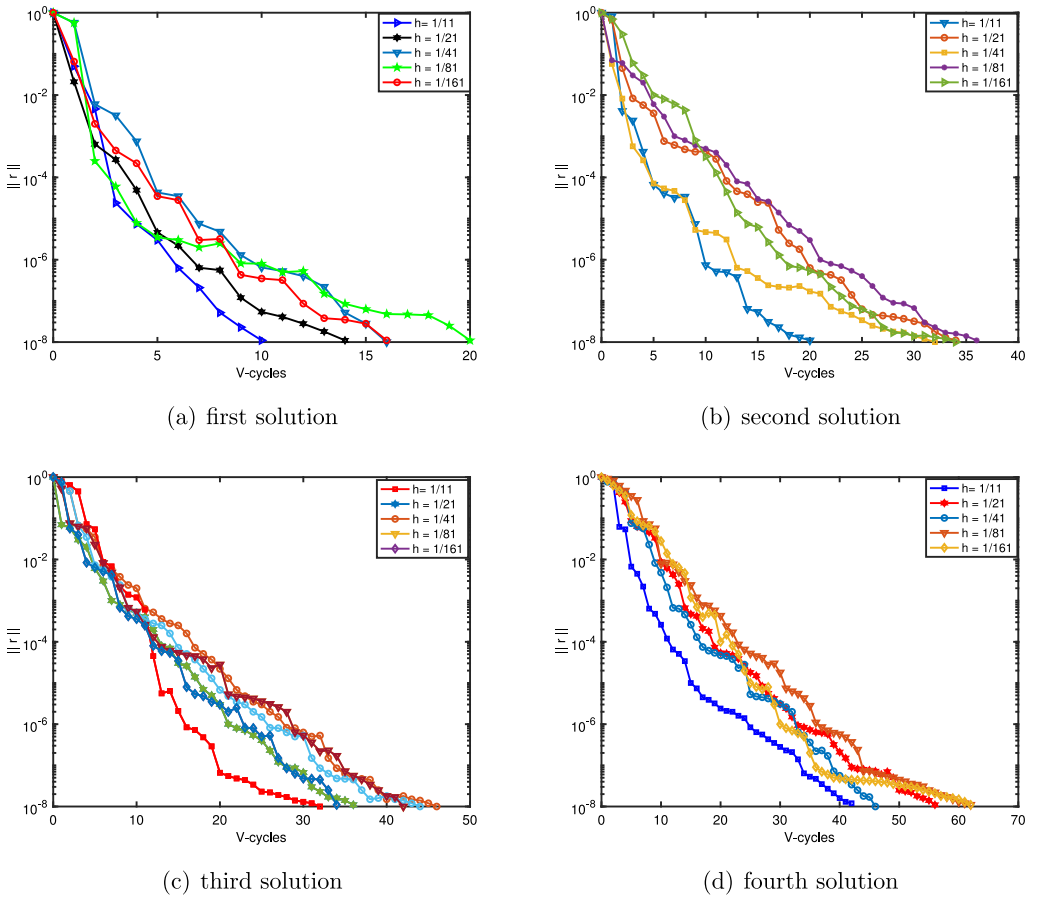

Fig. 7. Numerical convergence of the four solutions: u_1, u_2, u_3 and u_4, respectively, as a function of the number of V-cycles and grid size h for $\lambda = 6.0$ of the three-dimensional GB model (1).

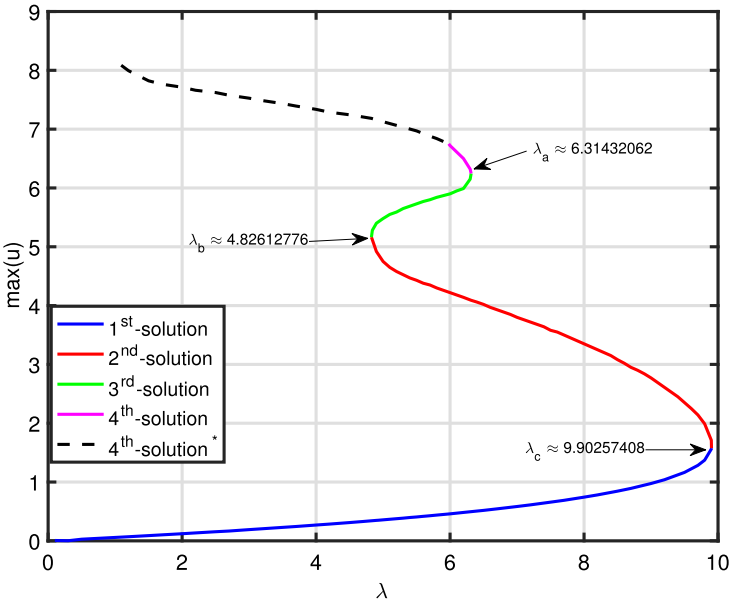

Fig. 8. Bifurcation curve for GB model (1) in three space dimensions. Solid lines indicate the four numerically converged solutions (see Fig. 7) and the dashed line shows spurious numerical solutions. The two new turning points $\lambda_a \approx 6.31432062$ and $\lambda_b \approx 4.8261277$. The third critical value $\lambda_c \approx 9.90257408$.

For the special choice of spherical coordinates, we find:

$$\begin{cases} x_1 = \rho\cos\phi_1, \\ x_2 = \rho\sin\phi_1\cos\phi_2, \\ x_3 = \rho\sin\phi_1\sin\phi_2\cos\phi_3, \\ x_4 = \rho\sin\phi_1\sin\phi_2\sin\phi_3\cos\phi_4, \\ \vdots \\ x_{n-1} = \rho\prod_{b=1}^{n-2}\sin\phi_b\cos\phi_{n-1}, \\ x_n = \rho\prod_{b=1}^{n-1}\sin\phi_b. \end{cases} \tag{9}$$

where $\rho > 0$, $0 \le \phi_b \le \pi$ $(b = 1, 2, 3, \ldots, n-2)$ and $0 \le \phi_{n-1} \le 2\pi$. The scaling coefficients in Eq. (8) are explicitly written as

$$\begin{cases} \zeta_1 = 1, \\ \zeta_2 = \rho, \\ \zeta_3 = \rho\sin\phi_1, \\ \vdots \\ \zeta_n = \rho\prod_{b=1}^{n-2}\sin\phi_b. \end{cases} \tag{10}$$

The Laplace operator (6) in n-dimensional spherical coordinates, making use of (8) and (9), becomes

$$\begin{aligned} \Delta = {} & \frac{1}{\rho^{n-1}}\frac{\partial}{\partial\rho}\left(\rho^{n-1}\frac{\partial}{\partial\rho}\right) \\ & + \frac{1}{\rho^2}\sum_{b=1}^{n-2}\left[\prod_{a=b+1}^{n-1}\frac{1}{\sin^2\phi_a}\left(\frac{1}{\sin^{b-1}\phi_b}\left(\frac{\partial}{\partial\phi_b}\sin^{b-1}\phi_b\,\frac{\partial}{\partial\phi_b}\right)\right)\right] \\ & + \frac{1}{\rho^2}\left(\frac{1}{\sin^{n-2}\phi_{n-1}}\frac{\partial}{\partial\phi_{n-1}}\left(\sin^{n-2}\phi_{n-1}\,\frac{\partial}{\partial\phi_{n-1}}\right)\right). \end{aligned} \tag{11}$$

For two dimensions (11) becomes

$$\Delta = \frac{1}{\rho}\frac{\partial}{\partial\rho}\left(\rho\frac{\partial}{\partial\rho}\right) + \frac{1}{\rho^2}\frac{\partial^2}{\partial\phi_1^2},$$

and for three dimensions

$$\Delta = \frac{1}{\rho^2}\frac{\partial}{\partial\rho}\left(\rho^2\frac{\partial}{\partial\rho}\right) + \frac{1}{\rho^2}\frac{1}{\sin^2\phi_2}\frac{\partial^2}{\partial\phi_1^2} + \frac{1}{\rho^2\sin\phi_2}\frac{\partial}{\partial\phi_2}\left(\sin\phi_2\frac{\partial}{\partial\phi_2}\right).$$

In the following section, we transform the nonlinear PDE (1) defined on the ball B, making use of the n-dimensional spherical coordinates.

5.2. A boundary-value problem in n-dimensional spherical coordinates

We rewrite the nonlinear problem (1) in n-dimensional spherical coordinates (9) as:

$$\begin{aligned} & \frac{1}{\rho^{n-1}}\frac{\partial}{\partial\rho}\left(\rho^{n-1}\frac{\partial u}{\partial\rho}\right) + \frac{1}{\rho^2}\sum_{b=1}^{n-2}\left[\prod_{a=b+1}^{n-1}\frac{1}{\sin^2\phi_a}\left(\frac{1}{\sin^{b-1}\phi_b}\left(\frac{\partial}{\partial\phi_b}\sin^{b-1}\phi_b\,\frac{\partial u}{\partial\phi_b}\right)\right)\right] \\ & \quad + \frac{1}{\rho^2}\left(\frac{1}{\sin^{n-2}\phi_{n-1}}\frac{\partial}{\partial\phi_{n-1}}\left(\sin^{n-2}\phi_{n-1}\,\frac{\partial u}{\partial\phi_{n-1}}\right)\right) + \lambda\,\mathrm{e}^u = 0. \end{aligned} \tag{12}$$

Next, we simplify partial differential equation (12) using symmetry properties. If Ω is a ball B in $\mathbb{R}^n$ centered at 0, then we could seek for radially symmetric solutions. More precisely, for $\Omega = B = \{\vec{x} \in \mathbb{R}^n : \|\vec{x}\|_2 < 1\}$, let $u \in C^2(\Omega, \mathbb{R})$ be a positive solution of (12), then u is radially symmetric (details can be found in [4]). This implies that the derivatives w.r.t. $\phi_1, \phi_2, \ldots, \phi_n$ are identically zero and Eq. (12) reduces to the ODE:

$$\frac{1}{\rho^{n-1}}\frac{\partial}{\partial\rho}\left(\rho^{n-1}\frac{\partial u}{\partial\rho}\right) + \lambda\,\mathrm{e}^u = 0. \tag{13}$$

For $\rho := \|\vec{x}\|_2$, we have $u = u(\rho) \in C^2[0,1]$ and $\frac{\partial u}{\partial \rho}(\rho) = u'(\rho) < 0$ for $\rho \in (0,1)$ (details are given in [4]). This implies that any positive solution of BVP (1) is a solution of the following ODE:

$$u'' + \frac{n-1}{\rho}u' + \lambda\, e^u = 0, \quad 0 < \rho < 1 \tag{14}$$

with boundary conditions $u'(0) = 0$ and $u(1) = 0$. In the next section, we discuss the multiplicity results and the bifurcation behaviour of nonlinear ODE (14) for different values of the dimension parameter n.

5.3. Theoretical results for n space dimensions in spherical coordinates

For ODE (14), theoretical results are given in [4] based on the dimension parameter n in the following way:

1. For $n = 1$, there exists a $\lambda_c > 0$ such that
   (a) for each $\lambda \in (0, \lambda_c)$, there are two solutions.
   (b) for $\lambda = \lambda_c$, there is a unique solution.
   (c) for $\lambda > \lambda_c$, there are no solutions.
2. For $n = 2$, define $\lambda_c = 2$. Then
   (a) for each $\lambda \in (0, \lambda_c)$, there are two solutions.
   (b) for $\lambda = \lambda_c$, there is a unique solution.
   (c) for $\lambda > \lambda_c$, there are no solutions.
3. For $3 \le n \le 9$, define $\tilde{\lambda} = 2(n-2)$. Then there exists a $\lambda_c > \tilde{\lambda}$ such that
   (a) for $\lambda = \lambda_c$, there is a unique solution.
   (b) for $\lambda > \lambda_c$, there are no solutions.
   (c) for $\lambda = \tilde{\lambda}$, there is a countable infinite of solutions.
   (d) for each $\lambda \in (0, \lambda_c)\backslash\{\tilde{\lambda}\}$, there is a finite number of solutions.
4. For $n \ge 10$, define $\lambda_c = 2(n-2)$. Then
   (a) for $\lambda \ge \lambda_c$, there are no solutions.
   (b) for $\lambda \in (0, \lambda_c)$, there is a unique solution.

We are going to numerically detect these solutions in the next section.

5.4. Numerical experiments

We compute the numerical solutions of the nonlinear ODE (14) by using a simple shooting method. For the numerical time-integration as a part of the shooting method, we use the MATLAB function *ode45* with a tolerance 10^{-10}. Several experiments are performed for different values of n. We present the bifurcation behaviour as a function of the parameter λ and the spatial dimension n. The bifurcation curves show the relation between $u(0)$ (maximum value of a solution) and $u(1)$. The numerical experiments confirm all theoretical results as mentioned in Section 5.3.

5.4.1. Experiment 1

We present numerical solutions of ODE (14) for $n = 1$ and different values of λ. Fig. 9 (left), illustrates the two numerical solutions u_1 and u_2 for $\lambda = 0.8$ and the unique solution u_c for λ_c. The critical value $\lambda_c \approx 0.86752074$ is calculated numerically. A bifurcation diagram for $n = 1$ of nonlinear ODE (14) for different values of λ is provided, see Fig. 9 (right), wherein the solutions can be identified as a zero of the curve $(u(0), u(1))$. These bifurcation curves show that for $0 < \lambda < \lambda_c$ there exist exactly two solutions, precisely one solution for $\lambda = \lambda_c$ and no solution exists for $\lambda > 0$.

5.4.2. Experiment 2

The numerical results of ODE (14) for $n = 2$ are now discussed. Two numerical solutions exist for $\lambda \in (0, \lambda_c)$ and one solution u_c for λ_c. These aspects are presented in Fig. 10. For this case, the critical value is $\lambda_c \approx 2$. We show the bifurcation behaviour in n space dimensions for ODE (14) with $n = 2$ and different values of λ. The curves in Figs. 11(a) and 11(b) show the maximum value of the two solutions: u_1, u_2 for $\lambda \in (0, \lambda_c)$, a unique solution for λ_c and no solution for $\lambda > \lambda_c$. This behaviour can be explained theoretically (see Section 5.3).

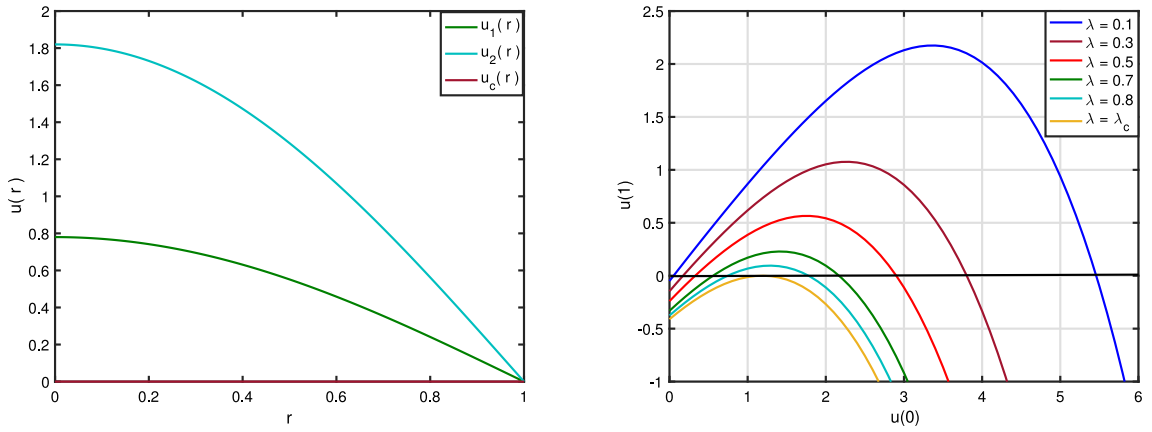

(a) Numerical solutions for $\lambda = 0.8$ and λ_c (b) Bifurcation curves for different values of λ.

Fig. 9. For the dimension parameter $n = 1$ in nonlinear ODE (14): two numerical solutions $u_1(r), u_2(r)$ for $\lambda = 0.8$ and one solution $u_c(r)$ for the critical value λ_c (left) and bifurcation curves for different values of λ (right).

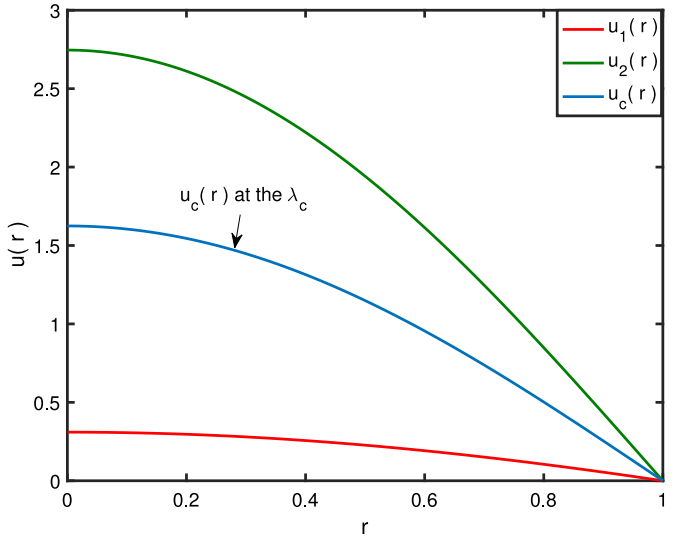

Fig. 10. Numerical solutions of nonlinear model (14) for $n = 2$: two solutions $u_1(r), u_2(r)$ for $\lambda = 1$ and one solution $u_c(r)$ for the critical value $\lambda_c = 2$.

5.4.3. Experiment 3

We provide numerical results of BVP (14) for $3 \leq n \leq 9$. The theoretical results for this case are quite different from the cases $n = 1$ and $n = 2$. We will show the existence of multiple solutions for different values of λ. As a characteristic example we take $n = 3$. For different values of λ, one, two, three or more solutions are depicted in Fig. 12. For $n = 3$, we have $\tilde{\lambda} = 2$. We compute several solutions for $\lambda \in (0, \lambda_c)\backslash\{\tilde{\lambda}\}$. For this, we take $\lambda = 1.999$ and computed the *seven* solutions, see in Fig. 12 (right). For this characteristic example, a unique solution u_c exists for critical value λ_c. The critical value for $n = 3$ is numerically found to be $\lambda_c \approx 3.352731$. The theoretical results for $3 \leq n \leq$ as described in Section 5.3, are confirmed numerically in Figs. 13 and 14 wherein a solution of ODE (14) for $n = 3$ can be identified as a zero of the curve $(u(0), u(1))$. The bifurcation behaviour for $n = 3$, is shown in Fig. 13 at $\tilde{\lambda} = 2$. Fig. 14 provides the bifurcation curves for $n = 4, 9$ respectively, for different values of λ.

5.4.4. Experiment 4

For numerical illustration of the case $n \geq 10$; we take the value $n = 10$ as a characteristic example. The numerical results can be found in Fig. 15. They again confirm the theoretical results as described in Section 5.3. For this example, we found the critical value $\lambda_c = 16$. A single solution exists for all values of $\lambda \in (0, \lambda_c)$ and bifurcation diagrams for the dimension parameter $n = 10$ are given in Fig. 15.

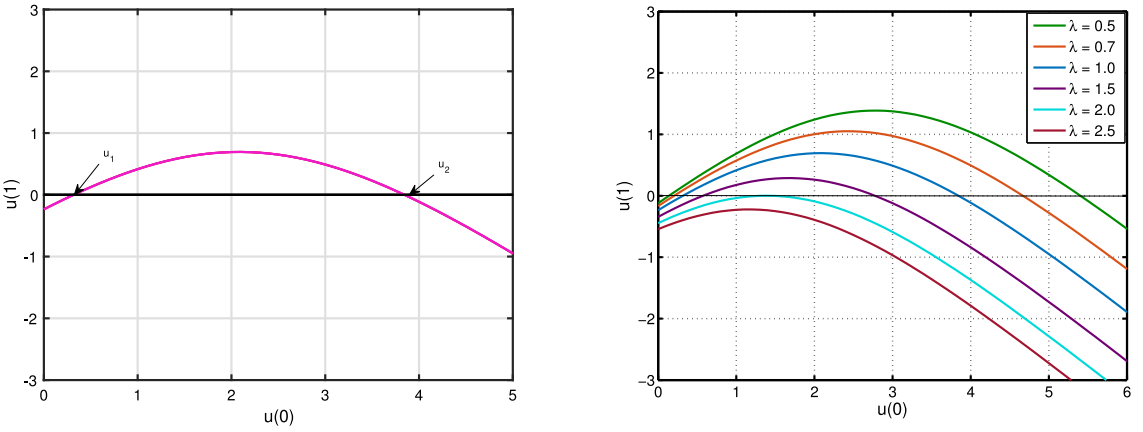

(a) Bifurcation curve for $\lambda = 1$. (b) Bifurcation curves for other values of λ.

Fig. 11. Bifurcation curves for $n = 2$ of model (14): two numerical solutions u_1, u_2 are identified as a zero of the curve $(u(0), u(1))$ for $\lambda = 1$ (left) and for the other values of λ (right).

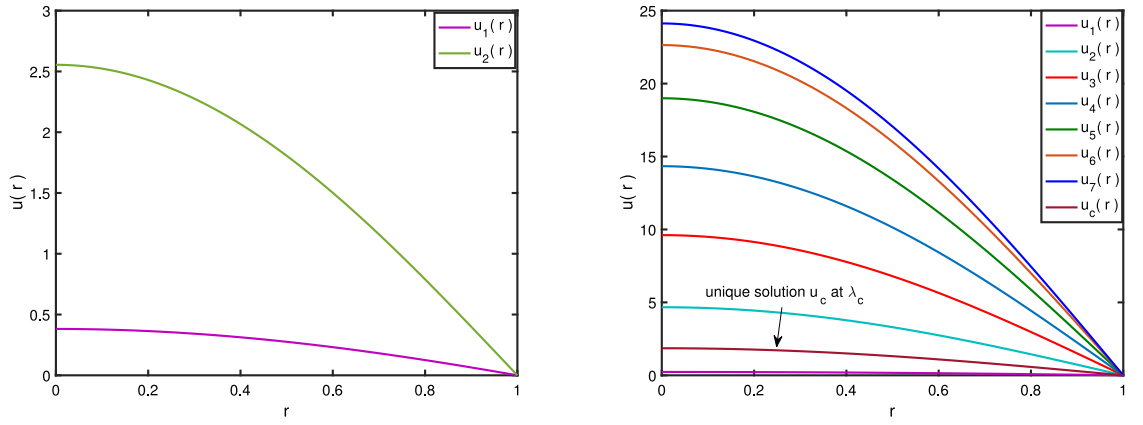

Fig. 12. Numerical solutions of nonlinear ODE (14) for $n = 3$. Two solutions: u_1, u_2 for $\lambda = 3$ (left). Multiple solutions for $\lambda = 1.999$ and one solution u_c for $\lambda_c \approx 3.352731$ (right).

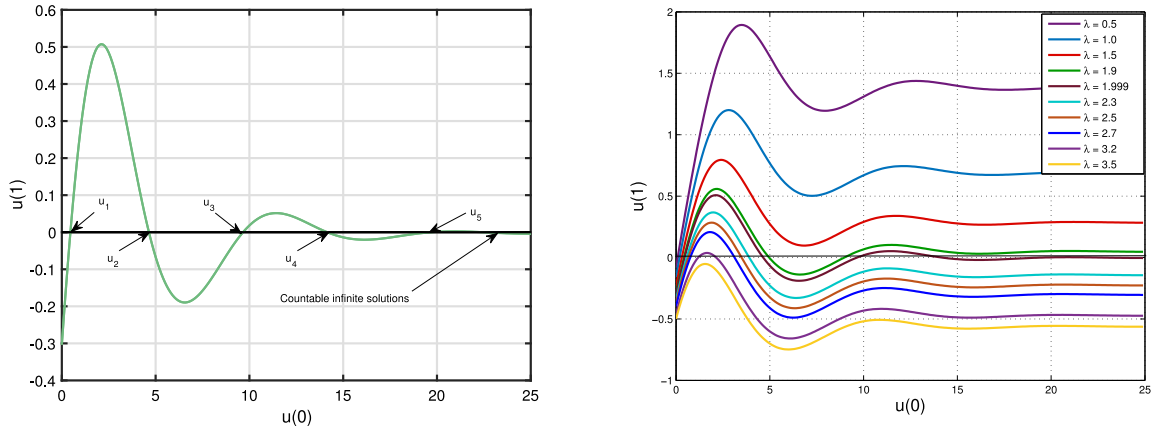

(a) (b)

Fig. 13. Bifurcation curves of model (14) for $n = 3$: multiple solutions $u_1, u_2, u_3, u_4, u5$ are identified as a zero of the curve $(u(0), u(1))$ for $\lambda = 2$ (left) with different values of λ (right).

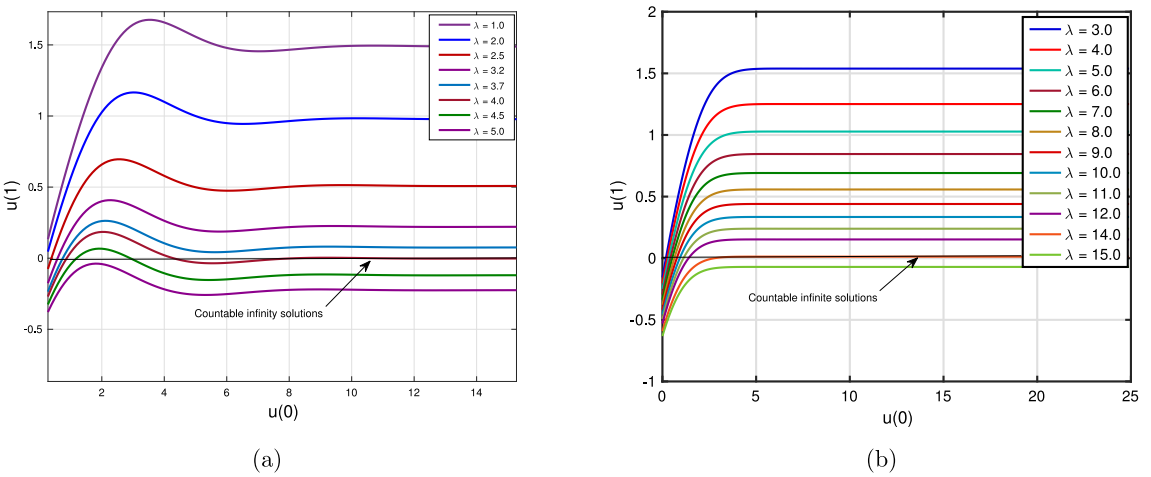

Fig. 14. Bifurcation curves for $3 \leq n \leq 9$ of nonlinear ODE (14): the cases for dimension parameter $n = 4$ (left) and $n = 9$ (right) respectively, with different values of λ.

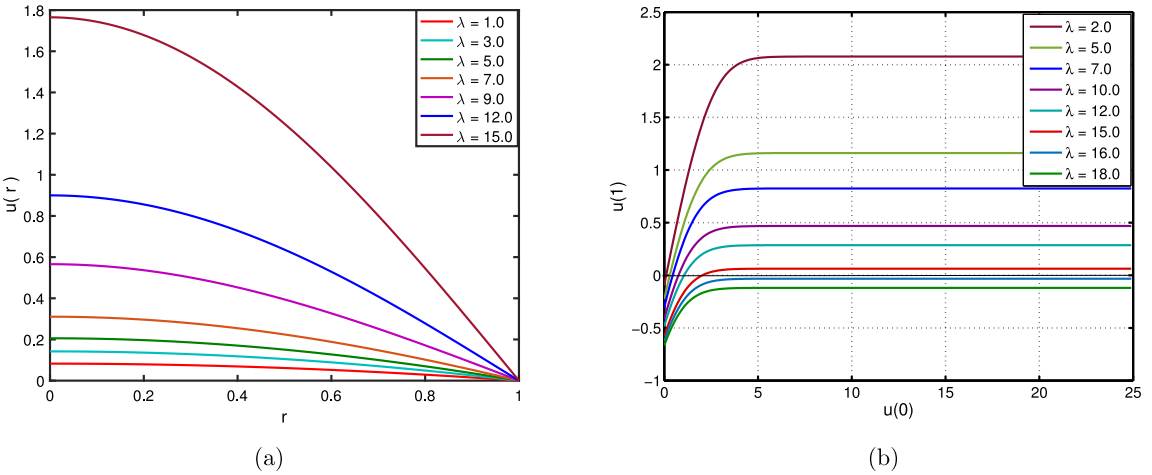

Fig. 15. Numerical results for dimension parameter $n = 10$ of nonlinear model (14) with different values of λ: one solution (left) and bifurcation curves (right).

6. Conclusion

In this article, we presented a numerical study of the Gelfand–Bratu model for higher dimensions. For three dimensions, we adopted an accurate and efficient nonlinear multigrid approach: the *full approximation scheme* (FAS) extended with a Krylov method as a smoother. In particular, we found new solutions for specific values of the bifurcation parameter. As known from the literature, finding new solutions and new turning points is a hard task. We indeed observed that the three-dimensional case is numerically much more complicated than the one-and two-dimensional cases. Furthermore, we extended the numerical bifurcation curve of the Gelfand–Bratu problem in three dimensions and showed the existence of two new turning points: λ_a and λ_b. Numerical results confirmed the convergence of all types of solutions (unique and multiple) and demonstrated the effectiveness of the proposed numerical strategy for all values of the parameter $\lambda \in (0, \lambda_c]$. For even higher dimensions, we transformed the Gelfand–Bratu problem using n-dimensional spherical coordinates to a single nonlinear ODE. We summarized a few theoretical results depending on the dimension parameter n and bifurcation parameter λ. Numerical solutions of this ODE were computed by a shooting method for a range of values of n. The experiments showed the existence of several types of solutions. Bifurcation curves for different values of n and λ confirmed the theoretical results of the higher dimensional Gelfand–Bratu problem as presented in literature.

Acknowledgement

Sehar Iqbal acknowledges the financial support by the Schlumberger Foundation (Faculty for the Future award).

References

[1] I.M. Gelfand, Some problems in the theory of quasi-linear equations, Uspekhi Mat. Nauk 14 (2) (1959) 87–158.
[2] G. Bratu, Sur l'équations intégrales exponentielle, C. R. Seances Acad. Sci. (1911) 1048–1050.
[3] G. Bratu, Sur les équations intégrales non linéaires, Bull. Soc. Math. France 42 (1914) 113–142.
[4] J. Bebernes, D. Eberly, Mathematical Problems from Combustion Theory, Applied Mathematical Sciences, vol. 83, Springer Science and Business Media, 2013.
[5] A.M. Wazwaz, Adomian's decomposition method for a reliable treatment of the bratu-type equations, Appl. Math. Comput. 166 (3) (2005) 652–663.
[6] S. Chandrasekhar, An Introduction to the Study of Stellar Structure, Vol. 2 , Dover Publications, INC, 1967.
[7] T.F.C. Chan, H.B. Keller, Arc-length continuation and multigrid techniques for nonlinear elliptic eigenvalues problems, SIAM J. Sci. Stat. Comput. 3 (2) (1982) 173–194.
[8] Y.Q. Wan, Q. Guo, N. Pan, Thermo-electro-hydrodynamic model for electrospinning process, Int. J. Nonlinear Sci. Numer. Simul. 5 (1) (2004) 5–8.
[9] I. Shufrin, O. Rabinovitch, M. Eisenberger, Elastic nonlinear stability analysis of thin rectangular plates through a semi-analytical approach, Int. J. Solids Struct. 46 (10) (2009) 2075–2092.
[10] M. Hajipour, A. Jajarmi, D. Baleanu, On the accurate discretization of a highly nonlinear boundary value problem, Numer. Algorithms 79 (3) (2018) 679–695.
[11] J. Karkowski, Numerical experiments with the Bratu equation in one, two and three dimensions, Comput. Appl. Math. 32 (2) (2013) 231–244.
[12] D.D. Joseph, T.S. Lundgren, Quasilinear Dirichlet problems driven by positive sources, Arch. Ration. Mech. Anal. 49 (4) (1973) 241–269.
[13] B. Gidas, W.M. Ni, L. Nirenberg, Symmetry and related properties via the maximum principle, Comm. Math. Phys. 68 (3) (1979) 209–243.
[14] J.S. McGough, Numerical continuation and the Gelfand problem, Appl. Math. Comput. 89 (1–3) (1998) 225–239.
[15] T. Washio, C.W. Oosterlee, Krylov subspace accerlation for nonlinear multigrid schemes, Electron. Trans. Numer. Anal 6 (1997) 271–290.
[16] A. Mohsen, L.F. Sedeek, S.A. Mohamed, New smoother to enhance multigrid-based methods for the Bratu problem, Appl. Math. Comput. 204 (1) (2008) 325–339.
[17] F. Jing-Jing, H. Ling, Y. Shi-Jie, Solutions of Laplace equation in n-dimensional spaces, Commun. Theor. Phys. 56 (4) (2011) 623–625.